# Electrochemical rapid reconstruction of 1D ZIF-L derived hollow hierarchical multiphase NiCo-S for high-performance hybrid supercapacitors

**SCHOLARONE™**
**Manuscripts**

**Electrochemical rapid reconstruction of 1D ZIF-L derived hollow hierarchical multiphase NiCo-S for high-performance hybrid supercapacitors**

Lin Sun, Fangrong Yan, Chunxiao Shi, Hang Wei, Yu Liu, Qingjun Yang, Runmei Luo, Guiquan Liu, Weidong Shi*

*School of Chemistry and Chemical Engineering, Jiangsu University, Zhenjiang 212013, PR China.*

*Corresponding Author*

*E-mail: swd1978@ujs.edu.cn*

*Tel: +86-511-88791800*

1

**Abstract**

The combination of low electronegative sulfur and common transition metals has obvious advantages in easing volume expansion and improving electrical conductivity for energy storage. Herein, we developed an electrochemically assisted strategy to rapidly reconstruct ZIFs (Zeolitic Imidazolate Frameworks) with Lewis acid to obtain reticulated cross-linked hierarchical electrode NiCo-LDH@CNFs (carbon-nitrogen frameworks) with excellent active specific surface area. Simple vulcanization can effectively optimize the active site and crystal structure, and further improve the conductivity of the multi-phase electrode NiCo-S@CNFs ($NiCo_2S_4$, $CoS_2$). Furthermore, the synergistic effect of multi-phase metal sulfides and the reasonable structure can effectually enhance the redox activity, adsorption capacity of $OH^-$, and reduce the volume expansion and of the electrode. The results demonstrate that the specific capacity of the electrode is 433.3 mAh $g^{-1}$ (6 M KOH). The prepared HSC device (hybrid supercapacitor, NiCo-S@CNFs//AC (activated carbon)) exhibits a maximum energy density of 87.2 Wh $kg^{-1}$ (800 W $kg^{-1}$). After 12,000 charge/discharge cycles, the capacity retention rate is still 105.1%, which has excellent cycling stability among ZIF-derived binary metal sulfides. Furthermore, parallel-connected LEDs can be lit by two series-connected HSCs, showing their practicality and great potential.

**Keywords:** ZIF-L derivatives; Electrochemical rapid reconstruction; Hierarchical structure; Multiphase NiCo-S synergy; Hybrid-supercapacitors

## 1. Introduction

Supercapacitors are widely applied in the new energy power and modern electronics industry as an energy storage/conversion device that can achieve high-efficiency charging/discharging processes with the advantages of long life and low cost[1-3]. Enhancing the energy density of capacitors and their cycling stability are the key factors to effectively promote their commercial application, and their cycling stability cannot meet the basic requirements at the high energy density available[4-6]. Therefore, constructing a stable structural system and enhancing the electrochemical performance of the active material are the main means of improvement at present.

In recent years, transition metal sulfides (TMSs) have demonstrated broad application prospects in transition metal active materials because of their remarkable redox activity and abundant adsorption active sites[7-8]. In particular, the low electronegativity of sulfur provides a solid basis for the structural stability and high mechanical flexibility of sulfides[9-10]. The conventional TMSs do not achieve their excellent theoretical specific capacity when tested in practice, and the possible problems are uncontrollable structure, poor electrode stability due to volume deformation, and conductivity reduction during the reaction process[11-12]. When the energy storage reaction is carried out, irreversible damage occurs to the electrode due to volume expansion and reduction in conductivity. As a consequence, when the energy density reaches 50 Wh kg$^{-1}$ (after 5000 charge/discharge cycles), the corresponding cycle stability performance is generally less than 90%[13-14]. Therefore, it is necessary to establish a stable structure to prevent the damage of the electrode material from the

3

decrease of electrical conductivity, to effectively improve its cyclic stability performance[15-16].

There are two key measures to solve the existing problems, one is to build a reasonable and stable structure to alleviate the volume expansion, and the other is to adjust the internal phase composition to obtain a multi-phase collaborative electrode system, further reducing the electrode resistance and increase the conductivity[17-20]. The construction of hollow hierarchical structures provides an excellent solution to this problem, and their special structure can effectively reduce the volume expansion of the electrodes, and optimize the conductivity of the electrodes[21-22]. Moreover, the skeleton of the nanoarrays with hollow hierarchical structures establishes electron transport channels, while the branching structure creates more ion storage sites, reducing the volume expansion effect of electrodes, and effectively improving the stability of electrodes[23-25]. In addition, adjusting the internal components to obtain a multi-phase composite non-homogeneous structure system, further reduces the electrode resistance, and effectively improves the conductivity and cycling stability of the electrode[26-27]. Qu et al. synthesized heterostructured electrode $NiCo_2S_4@NiS$ with the hollow core-shell structure on carbon fibers and obtained higher energy density (62.4 Wh kg$^{-1}$) and significantly higher stability, and capacity retention up to more than twice that of the precursor (after 5000 cycles)[28]. Hence, more efficient and integrated construction of complex nanostructured systems with enhanced activity and stability of electrodes remains our main problem.

Herein, we successfully synthesized hollow hierarchical multiphase NiCo-S@CNFs

4

(carbon-nitrogen frameworks) composites based on reconstructing and modifying ZIF-L (Zeolitic Imidazolate Framework-L) by electrochemically assisted means and vulcanization. The electrodes have a high specific capacitance performance (433.3 mAh g$^{-1}$, 1 A g$^{-1}$), and their composition into supercapacitors (HSCs, NiCo-S@CNFs/CC//activated carbon (AC)), obtaining a high energy density (87.3 Wh kg$^{-1}$, 800 W kg$^{-1}$) and excellent stability. The remarkable cycling stability performance (105.1% after 12000 cycles) was achieved at higher energy density (more than 80 Wh kg$^{-1}$) among ZIF-derived binary metal sulfides. Furthermore, the reasonable hierarchical structure effectively reduces the volume expansion phenomenon, the multi-phase active material can further reduce the internal resistance, increase the conductivity, and effectively improve its electrochemical performance and stability. This work provides ideas for the efficient integration of building hierarchical structures and heterogeneous multiphase systems with enhanced stability.

## 2. Experiment section

The Materials and Physical Characterization section is in Supplemental Materials.

### 2.1. Synthesis of one-dimensional ZIF-L nanoarrays on CC

One-dimensional ZIF-L (CoZ1D) nanoarrays were prepared with an in-situ deposition strategy (~25 °C). 0.291 g of Co(NO$_3$)$_2$·6H$_2$O was added to 40 mL of deionized water (DIW) as solution A and 1.3136 g of 2-MI was also added to 40 mL of DIW as solution B, and the solution was completely dissolved by ultrasound. A piece of 1 × 2 cm$^2$ carbon cloth (sonicated with acetone, ethanol, and DIW) was quickly placed into the mixed solution of solutions A and B. Remove it after 8 hours at room

5

temperature (~25 °C), wash with DIW, and dry at 70 °C in a drying oven. The loading mass of precursor ZIF-L nanoarrays on CC was 1.5 mg cm$^{-2}$.

## 2.2. Synthesis of hierarchical structure nanoarrays NiCo-LDH on ZIF-L

NiCo-LDH was prepared by in situ electrochemically assisted rapid reconstruction (ion exchange/etching) performed simultaneously, resulting in a stable hierarchical structure. Dissolve 0.969 g Ni(NO$_3$)$_2$·6H$_2$O and 0.4845 g Co(NO$_3$)$_2$·6H$_2$O in 50 mL of DIW, and dissolve by ultrasonic. At -1.2 V, with a three-electrode system consisting of Ag/AgCl (reference electrode, RE), platinum (counter electrode, CE), and CoZ1D (working electrode, WE), NiCo-LDH nanosheets were prepared at 200 s, 300 s, and 400 s, respectively. Remove the sample to wash, and dry at 70 °C. The loading mass of intermediate NiCo-LDH@CNFs on CC was 2.0-2.5 mg cm$^{-2}$. In addition, electrolytes with different mass ratios (mNi + mCo=1.4543g, Ni: Co=1:0, 2:1, 1:1) were prepared to obtain samples with the best morphologies and properties, which were named NiCo-1: 0, NiCo-2:1 and NiCo-1:1.

## 2.3. Synthesis of hollow multiphase NiCo-S@CNFs/CC

Synthesis of hierarchical multiphase metal sulfides by a simple solvothermal method. The obtained precursors were transferred into a 50 mL polytetrafluoroethylene reactor, 20 mL of ethanol (C$_2$H$_5$OH) and 100 mg of thioacetamide (CH$_3$CSNH$_2$, TAA) were added, and placed in the oven for 2 h (120 °C). Then, the samples were taken out, washed, and dried at 70 °C, named NiCo-S-100-2. The most suitable reaction conditions were obtained by vulcanization, and the effect on the sample was studied by changing the time and concentration of vulcanization. The reaction times (1 h, 3 h) were

6

respectively named NiCo-S-100-1 and NiCo-S-100-3. Under the condition of reaction

time, the amount of TAA added (50 mg, 150 mg) was changed, the samples were named

NiCo-S-50-2 and NiCo-S-150-2, and the best vulcanization conditions were obtained.

The loading mass of active substance NiCo-S@CNFs on CC was 2.5-3.0 mg cm$^{-2}$.

## 3. Results and discussion

### 3.1. Morphology and material analysis

The synthesis procedure of the hollow hierarchical multiphase NiCo-S@CNFs array
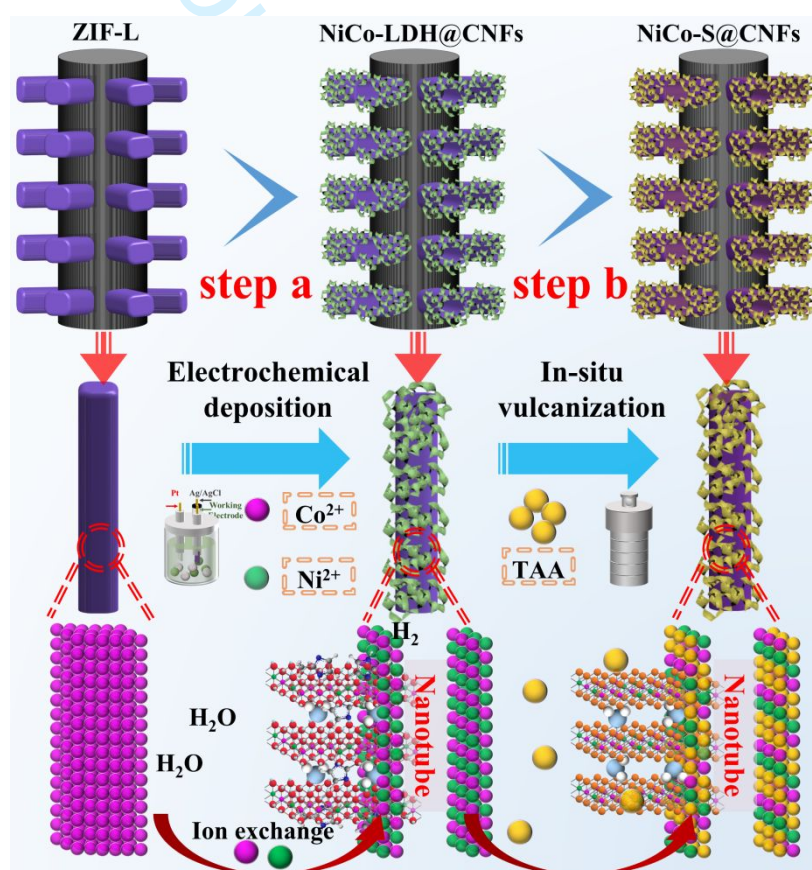
is shown in Fig. 1.



**Fig. 1.** The synthesis route illustration of hierarchical electrode NiCo-S@CNFs in-situ grown and

regulation on carbon cloth (CC).

With a room temperature in-situ auto-deposition method, the original 1D ZIF-L array

was synthesized. The structure of 1D ZIF-L was protected and reconstructed to obtain

7

hollow-CNFs by electrochemically assisted fast and efficient ion exchange and etching to form a hollow hierarchical structure (NiCo-LDH@CNFs, step a). The hollow hierarchical structure provides a suitable platform for the preparation of the multiphase active substance, which effectively promotes the reaction kinetics of the electrical level, resulting in highly stable electrodes. Finally, through sulfidation, metal sulfides of different phases are obtained, and the NiCo-S@CNFs electrode is realized (step b).

In Fig. 2a, the crystallinity of the intermediate NiCo-LDH/ZIF-L and the active material multiphase NiCo-S@CNFs crystal phase was determined by XRD. Most of the ZIF-L peaks are still retained in the XRD pattern (intermediate NiCo-LDH/ZIF-L) [29], meanwhile, (009), (012), (015), and (113) reflect the planes of the NiCo-LDH phase crystal planes, indicating their successful preparation[30]. When electrochemically modified efficiently and rapidly, the structure of ZIF-L is preserved and its components are maintained, forming a hollow hierarchical structure with different phases inside and outside. After vulcanization, the ZIF-L and NiCo-LDH peaks in the spectrum disappeared, and new obvious diffraction peaks appeared. Among them (111), (200), (210), (211), and (222) correspond to the characteristic peaks of 27.9 $^{\circ}$, 32.3 $^{\circ}$, 36.2 $^{\circ}$, 39.8 $^{\circ}$, 57.6 $^{\circ}$, and $CoS_2$ (JCPDS No. 41-1471). Besides, (111), (220), (400), (440) correspond to 16.3 $^{\circ}$, 26.8 $^{\circ}$, 38.3 $^{\circ}$, and 55.3 $^{\circ}$, which are characteristic peaks of $NiCo_2S_4$ (JCPDS No. 20-0782)[31-33]. The spectra indicate the successful preparation of the multiphase synergistic active species NiCo-S@CNFs. The XPS test studies the chemical properties and bonding changes of electrodes by measuring the binding energy of electrons. The characteristic peaks corresponding to each element are

8

displayed in the XPS comparison spectrum (Fig. 2b), and the characteristic peaks of S appear in the spectrum after vulcanization, indicating that the sample NiCo-LDH@CNFs and NiCo-S@CNFs (optimal electrode) are successfully synthesized. In Fig. 2c, Co 2p has two spin-orbit doublets, in which the two characteristic peaks at the binding energies of 778.6 and 793.6 eV are consistent with $Co^{3+}$, while the peaks at 780.9 and 796.5 eV match with $Co^{2+}$, and the peaks at 786.2 and 803.0 eV is the satellite peak of Co 2p (identified as Sat.)[34-35]. In the Ni 2p orbital (Fig. 2d), the two primary characteristic peaks at 853.2 (Ni $2p_{3/2}$) and 870.4 eV (Ni $2p_{1/2}$) in the spectrum belong to $Ni^{2+}$, while the peaks at 855.9 and 873.9 eV belong to $Ni^{3+}$, its satellite peaks are 860.9 and 880.5 eV, respectively[36-37]. There are mixed valence states of $Co^{2+/3+}$ and $Ni^{2+/3+}$ in the multiphase active electrode, and the existence of multivalent states can improve the redox ability, thus improving the electrode activity. As shown in Fig. 2e, the XPS spectrum of S 2p is divided into three peaks, of which the peak at 162.2 eV matches with the low-coordination sulfide ion (S $2p_{3/2}$), and the 163.7 eV belongs to the metal-sulfur bond (S $2p_{1/2}$), indicating the existence of $S^{2-}$, which corresponds to the satellite peak at 168.6 eV[38-39]. In Fig. 2f-g, the nuclear energy level spectrum of C 1s is divided into characteristic peaks of 284.4, 285.8, and 287.7 eV (C-C, C-N, and C=O-C), while the spectrum of N1s, divided into 399.0, 400.1 and 401.1 eV (Pyridinic-N, Pyrrolic-N, and Graphitic-N), which confirmed the existence of CNFs[40-41]. The O 1s nuclear level spectrum in Fig. 2h is divided into three peaks M-O bond (530.6 eV), hydroxyl (531.5 eV), and absorbed oxygen (532.5 eV)[32]. By analyzing the element presence and bonding mode of electrode materials in the XPS diagram, we confirmed

9

the synthesis of NiCo-S@CNFs, which identified a foundation for an in-depth study of electrode activity. In addition, it was shown by $N_2$ adsorption/desorption that the multiphase electrode NiCo-S@CNFs has an outstanding BET-specific surface area and abundant pore structure, which provides a theoretical basis for demonstrating its excellent electrochemical performance (Fig. 2i).
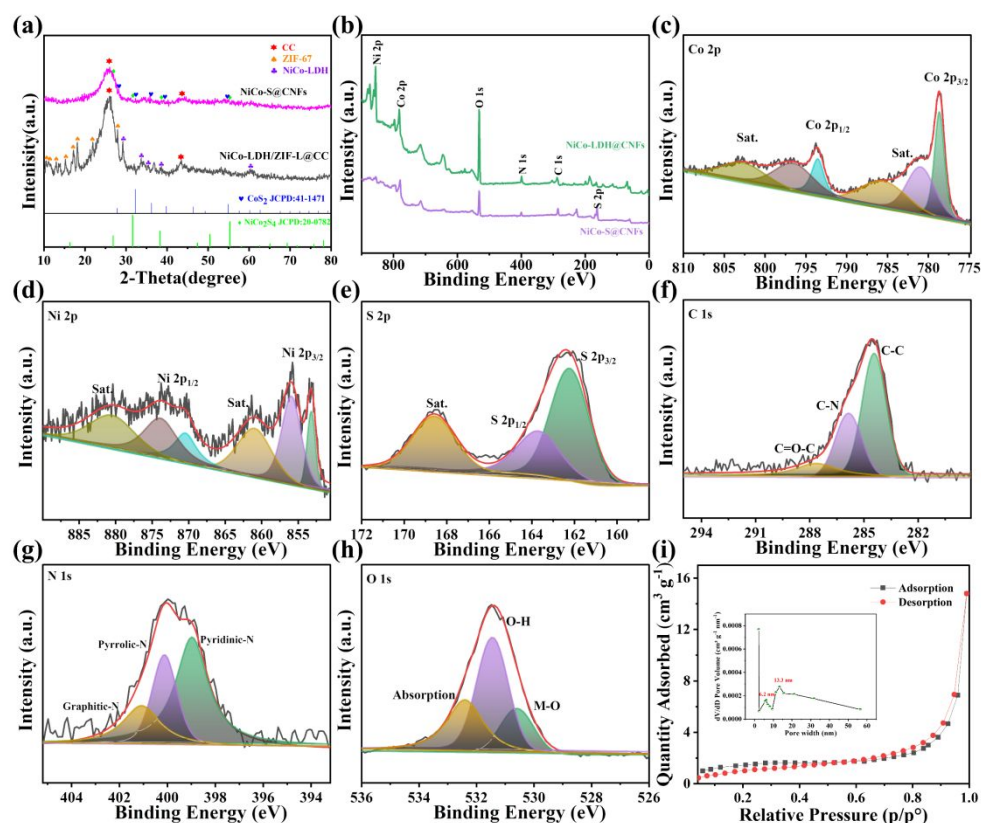


**Fig. 2.** XRD comparison patterns (a) and XPS survey spectra (b) of the precursor NiCo-LDH and the optimal sample NiCo-S@CNFs, XPS spectra of NiCo-S@CNFs: Co 2p (c), Ni 2p (d), S 2p (e), C 1s (f), N 1s (g), O 1s (h) and BET plots (i).

The design of a reasonable structure is the main point for enhancing the performance/stability of the electrode. Through the morphology analysis of the sample, the nanostructure characteristics of the sample are observed, and the electrode with a reasonable structure is constructed. First, 1D ZIF-L arrays were synthesized (Fig. 3a),

and they were neatly arranged on carbon fibers (uniform in size and stable in structure).

Fig. 3b shows the synthesis of 2D NiCo-LDH NSs (nanosheets) directly on carbon fibers by electrochemical-assisted means. The resulting nanosheets are large and unevenly distributed, resulting in easy shedding of the active material. Next, ZIF-L nanoarrays were reconstructed (electrochemically assisted etching and exchange), in which the 1D ZIF-L formed a hollow structure, the 2D NiCo-LDH NSs were uniformly distributed on the ZIF-L array, the precursor material NiCo-LDH@CNFs with a hollow hierarchical structure was obtained (Fig. 3c, Fig. S2-1). Combined with XRD, the 1D ZIF-L array still exists in the precursor, and the 2D nanosheets act as branched structures to protect its structure and effectively increase the specific surface area of the electrode, leading to much higher electrode performance. Finally, the precursors were vulcanized by the alcohol thermal method. The composition of the inner and outer layers of the precursor was different, and the NiCo-S@CNFs (CoS$_2$, NiCo$_2$S$_4$) with a multi-phase synergistic hollow hierarchical structure were obtained after vulcanization respectively (Fig. S2-2). By testing the energy spectrum line scans of the precursor and final samples, a clear hollow structure and differences in the elemental distribution between the inner and outer material can be observed (Fig. S2-3). Besides, the reasonable structure configuration provides an efficient platform to synthesize multiphase active material during the vulcanization process. Moreover, the hierarchical structure and multiphase synergy can enhance the capacity and stability. When the vulcanization time is 1 h (Fig. 3d), the composite structure can still be maintained, and an obvious hollow structure can still be found. When the vulcanization time is 2 h (Fig.

3e), the thickness of the nanosheets further increased, and the active materials of different phases synergized and reduced the resistance of the electrodes, resulting in a high-performance/stable electrode. When the vulcanization time is 3 h (Fig. 3f), the nanosheets are too thick, and the interconnected stacking phenomenon occurs, accompanied by the appearance of small particles, which hinder the electron transfer and reduce the electron transfer rate/electrode conductivity, leading to a decrease in electrode performance. In addition to considering the effect of vulcanization time on the electrode, the effect of adding different amounts of thioacetamide (TAA, 50 mg, 150 mg) on the electrode was investigated. The same pattern was presented with the increase of sulfidation time, with the increase of TAA amount, the thickness of nanosheets gradually increased and the degree of sulfidation deepened (Fig. S1e-f). Through systematic research, it is found that the difference in the degree of sulfidation (time, concentration) will affect the formation of active materials and the construction of reasonable structures, thereby changing their electron transport rate/conductivity and stability, and finally affecting the performance of the electrode. Next, under the same sulfidation conditions, the changes in electrode structure and morphology under different conditions during electrochemical reconfiguration were systematically investigated. The mass proportion of Ni and Co was adjusted in the electrolyte to study its effect on the structure, morphology, and performance of the electrode. When Ni: Co=1:1 (Fig. S1a), the active substance with the coexistence of 2D nanosheets and small particles is formed. Due to the uneven formation of nanosheets, the nanosheets fall off, and the 1D ZIF-L array is directly vulcanized to form sulfide. When Ni: Co=1:0

12

vulcanization (Fig. S1b), disordered and netted morphology is observed, which is because after electrochemical reconstruction, the particle matter attached to the 1D ZIF-L array is obtained, destroying the structure of the inner layer material and ultimately the overall structure. Moreover, different morphologies of electrodes can be obtained with different retention times in different electrochemical reconstruction processes. When the retention time was 200 s (Fig. S1c), the 2D NiCo-LDH NSs were only formed on the surface, forming nanosheets of smaller size and wrinkled shape, which formed fine active material particles after surface vulcanization. When the retention time is 400 s (Fig. S1d), the immersion time is too long under a high concentration of electrolyte and high voltage, resulting in excessive etching, the 1D ZIF-L structure is destroyed, and the result of excessive sulfidation occurs. It is observed that the elements are uniformly distributed in the structure of the composite material, and the hollow hierarchical structure improves the electron transport rate. Besides, element mapping and EDS spectrum of the electrodes before and after the durability test (Fig. S2) were provided. It can be seen from the element mapping that the elements (C, N, O, Ni, Co, S) of the sample NiCo-S@CNFs still exist and are uniformly dispersed after the durability test. Therefore, there is a certain amount of K, and the corresponding elements have obvious characteristic peaks in the EDS spectra, which is consistent with the fact, indicating that the original phase sulfide still exists after the durability test. Compared with the samples before the durability test, the O content increased significantly and the S content decreased correspondingly, which was consistent with the fact that the intermediates NiS-O and CoS-O were produced during the
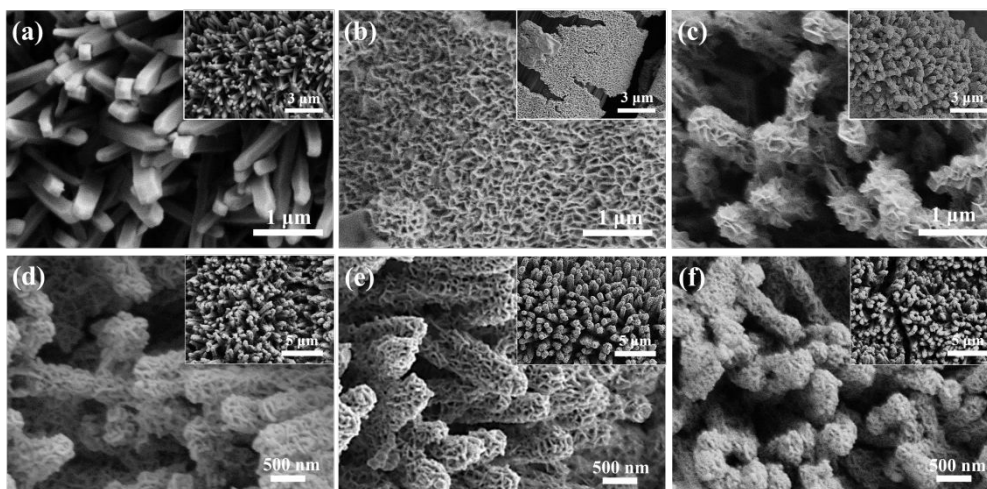
13

electrochemical redox process.



**Fig. 3.** SEM images at different magnifications: (a) ZIF-L, (b) NiCo-LDH NSs, (c) NiCo-LDH@CNFs; Morphologies of multiphase electrodes obtained by vulcanization at different times: (d)1 h, (e) 2 h, (f)3 h.

To further study and analyze the microstructure of the electrodes and to determine its material composition, TEM and HRTEM images (NiCo-S@CNFs) of the electrode were characterized, and its element diffraction pattern (Ni, Co, S, N, C, O) was obtained. As shown in Fig. 4a-f, the 2D nanosheets were attached as the main body to the 1D hollow carbon and nitrogen skeleton, forming a fine nanostructure. The construction of a reasonable structure could add a specific surface area, provide an electron transport channel, and effectively improve the electrochemical performance of the electrode. The HRTEM image of the NiCo-S@CNFs (Fig. 4g), where the lattice spacings of 0.2380 nm and 0.2769 nm are matched to the (311) plane of $NiCo_2S_4$ and the (200) plane of $CoS_2$, respectively[42-44]. This result shows that the crystal structure and material component of the electrodes were identified, demonstrating the successful synthesis of heterogeneous sulfides. Multi-metal multi-phase active materials make up for the

14

shortage of single-metal single-phase materials, provide more active sites for electrodes, and significantly improve electrode performance through synergistic effects. In addition, the distribution of elements in the electrode was shown by TEM mapping (Fig. 4h), and the active material was successfully synthesized and uniformly distributed.



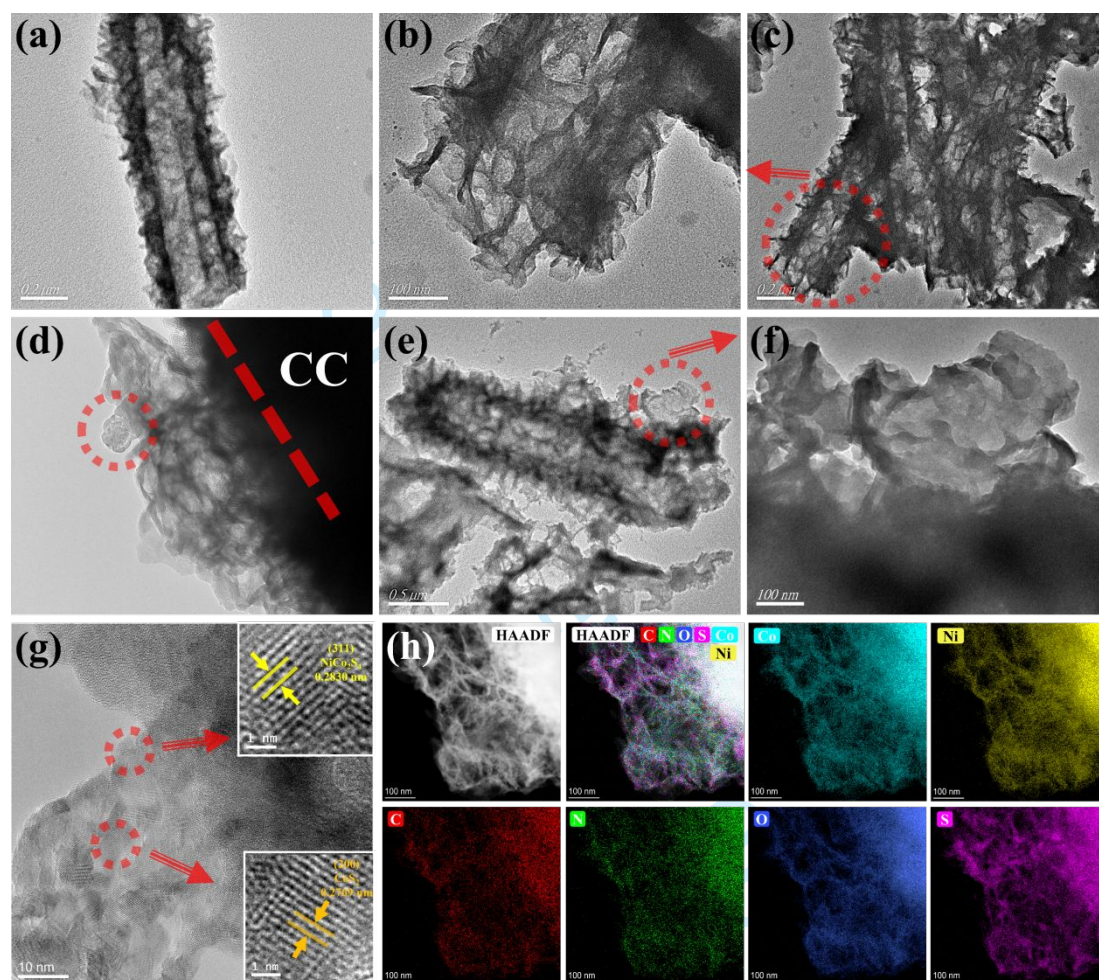**Fig. 4.** TEM images (a-f), HRTEM (g), and elemental (C, N, O, S, Co, Ni) maps (h) of multiphase electrode NiCo-S@CNFs.

## 3.2. Electrochemical tests

The electrochemical data and the performance analysis obtained by electrochemical tests are important for judging the quality of electrodes. In detail, the electrochemical results of the electrodes were obtained from the analysis of CV (cyclic voltammetry),
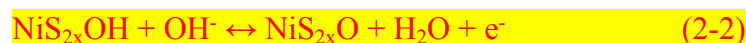
15

GCD (galvanostatic charge and discharge), and EIS (electrochemical impedance spectroscopy) curve (6 M KOH, 3 and 2-electrode system). The electrochemical performance of CoZ1D, NiCo-LDH@CNFs, and NiCo-S@CNFs were compared. Fig. 5a demonstrates that the CV curve for a voltage window is 0-0.5 V at a scan rate of 2 mV s$^{-1}$, and the integral area of the NiCo-S@CNFs curve is significantly larger than other curves, which proves the successful synthesis of the active material. Fig. 5d presents the GCD diagram at 1 A g$^{-1}$ (0-0.5 V), whose charge-discharge times reflect the capacity of the electrodes. Calculate its specific capacitance C$_s$ under different current densities according to the formula[45]

$$C_m = \int I \, dt / (m_o \times 3.6) \qquad (1\text{-}1)$$

$$C = Q / (m_o \times \Delta V) = \int I \, dt / (m_o \times \Delta V) \qquad (1\text{-}2)$$

where C$_m$, and C are the specific capacity (mAh g$^{-1}$), and mass-specific capacity (F g$^{-1}$), respectively, I, t, and $\Delta V$ are the discharge current(A), is the time(s), time, and voltage drop (V), respectively. The specific capacitances of CoZ1D, NiCo-LDH@CNFs, and NiCo-S@CNFs were calculated to be 33.3, 302.8, and 433.3 mAh g$^{-1}$ at 1 A g$^{-1}$, respectively, and compared with the precursor, the capacity of the final sample is significantly improved. The specific capacitances obtained for NiCo-S@CNFs at scan rates of 1, 2, 3, 5, 8, and 10 A g$^{-1}$ are 433.3, 411.1, 389.2, 352.4, 324.0, and 311.9 mAh g$^{-1}$, respectively. Attributed to the design of the hollow hierarchical structure could make full contact between the active material and electrolyte, speeding up the electron transport rate, and the two phases (NiCo$_2$S$_4$, CoS$_2$) synergize to obtain an electrode with superior performance. In addition, comparing the electrochemical

16

performance of the present working electrode with previously reported research work has obvious advantages (Table S1). When electrochemical tests were performed, the calculated specific capacity gradually decreased with increasing current density, and the NiCo-S@CNFs were structurally stable and exhibited good/stable rate capability (Fig. 5g), with capacity retention remaining at 73.4 %. By measuring the change of impedance with frequency, the impedance map (EIS, Fig. 5j) was obtained, and the capacitive behavior of the electrode (electrode process kinetics and diffusion mechanism) was further studied. In the high-frequency region, the intercepts of CoZ1D and NiCo-S@CNFs electrodes are similar to the real axis intercepts, which are much smaller than those of NiCo-LDH@CNFs electrodes, indicating that the volume resistance can be effectively reduced by vulcanization treatment. In the low-frequency region, the slope of the curve is larger, the charge transfer rate between the electrolyte and the electrode is faster, and the impedance is smaller. These tested structures demonstrate that the synthesis of hollow hierarchical structured multiphase sulfide electrodes is an effective means to enhance electrochemical performance. The redox reactions of the active materials are shown below[46-47]:

$$NiCo_2S_4 + 2OH^- \leftrightarrow NiS_{2x}OH + 2CoS_{2-x}OH + 2e^- \qquad (2\text{-}1)$$

$$NiS_{2x}OH + OH^- \leftrightarrow NiS_{2x}O + H_2O + e^- \qquad (2\text{-}2)$$

$$CoS_{2-x}OH + OH^- \leftrightarrow CoS_{2-x}O + H_2O + e^- \qquad (2\text{-}3)$$

$$CoS_2 + OH^- \leftrightarrow CoS_2OH + e^- \qquad (2\text{-}4)$$

$$CoS_2OH + OH^- \leftrightarrow CoS_2O + H_2O + e^- \qquad (2\text{-}5)$$

To evaluate the improvement parameters in the vulcanization process, the

17

vulcanization time and the amount of TAA added were changed respectively, and it was named NiCo-S-100-2 according to the reaction conditions (100 represents the amount of TAA added (mg), 2 represents the reaction time (h)). Among them, when the amount of TAA added was 100 mg and the reaction time was 2 h, it was observed that the CV curve integrated area was the largest (Fig. 5b). In the GCD curve (Fig. 5e), the calculated specific capacitances at 1 A g$^{-1}$ for NiCo-S-100-1, NiCo-S-100-3, NiCo-S-50-2, and NiCo-S-150-2 are 414.7, 379.7, 289.9, and 305.8 mAh g$^{-1}$, all smaller than NiCo-S-100-2 (433.3 mAh g$^{-1}$). Although the performance at a reaction time of 1 h is only slightly lower than 2 h, there is a large gap in rate performance. Its specific capacitance was calculated by varying the scan rate (1 A g$^{-1}$ to 10 A g$^{-1}$), and NiCo-S-100-1, NiCo-S-100-3, NiCo-S-50-2, and NiCo-S-150-2 rate performance were 56.7%, 70.1%, 89.0%, and 73.6%, respectively (Fig. 5h). With the deepening of the vulcanization degree (the increase of vulcanization time and concentration), the active material is gradually formed. When the degree of vulcanization is low, it is in a state of transition to the active material, and the performance is improved to a certain extent. However, the degree of sulfidation gradually deepens, the active material is over-sulfurized, and the active material is stacked and accumulated, making it impossible to make full contact with the electrolyte, leading to a decrease in electrochemical performance. Further study of the impedance of the electrode, drawing the impedance spectrum for analysis (Fig. 5k), the NiCo-S-100-2 has a smaller volume resistance (intersection with the real axis) and diffusion resistance (slope). It is because by controlling the degree of vulcanization, the electrolyte can be fully contacted with the

18

active material (large specific surface area), providing an electron transport channel for the system, accelerating the electron transport rate, and obtaining electrodes with the best performance and lower impedance. Therefore, different reaction conditions were changed, the vulcanization process was optimized, and the best samples were obtained by combining morphology analysis and electrochemical testing. Modification of ZIF-L utilizing electrochemical remodeling is a key factor and an important condition for electrode formation. The optimal intermediate is obtained by changing the proportion of metal ions and time of electrochemical deposition, named NiCo 2:1-300-S (2:1 represents the ratio of NiCo, and 300 represents the time (s) of electrochemical deposition). Fig. 5c, f, i, 1 shows the comparative electrochemical tests after vulcanization of intermediates with different metal ratios. The discharge time of NiCo 2:1-300-S is significantly better than other conditions and has the lowest impedance, with the best electrochemical performance. When the electrochemical deposition time is too short, the modification and reconstitution of ZIF-L are limited and the performance enhancement is limited. In contrast, a too long time can severely damage the structure of ZIF-L or lead to the accumulation of reactive substances, resulting in significant performance degradation. The reaction conditions during electrochemical reconstitution were systematically studied, and the sample with the optimal electrochemical parameters was gained through electrochemical test analysis and comparison. In addition, the supporting information is supplemented with the CV, GCD spectrum, and rate performance spectrum (Fig. S3-S5). Besides, the specific capacity values in detail, coulomb efficiency of the samples at different current densities, rate

19

<mark>performance of the samples (1-10 A g$^{-1}$), the EIS fitted data for all the EIS graphs are shown in the Supplementary Materials (Table S2-S7).</mark>
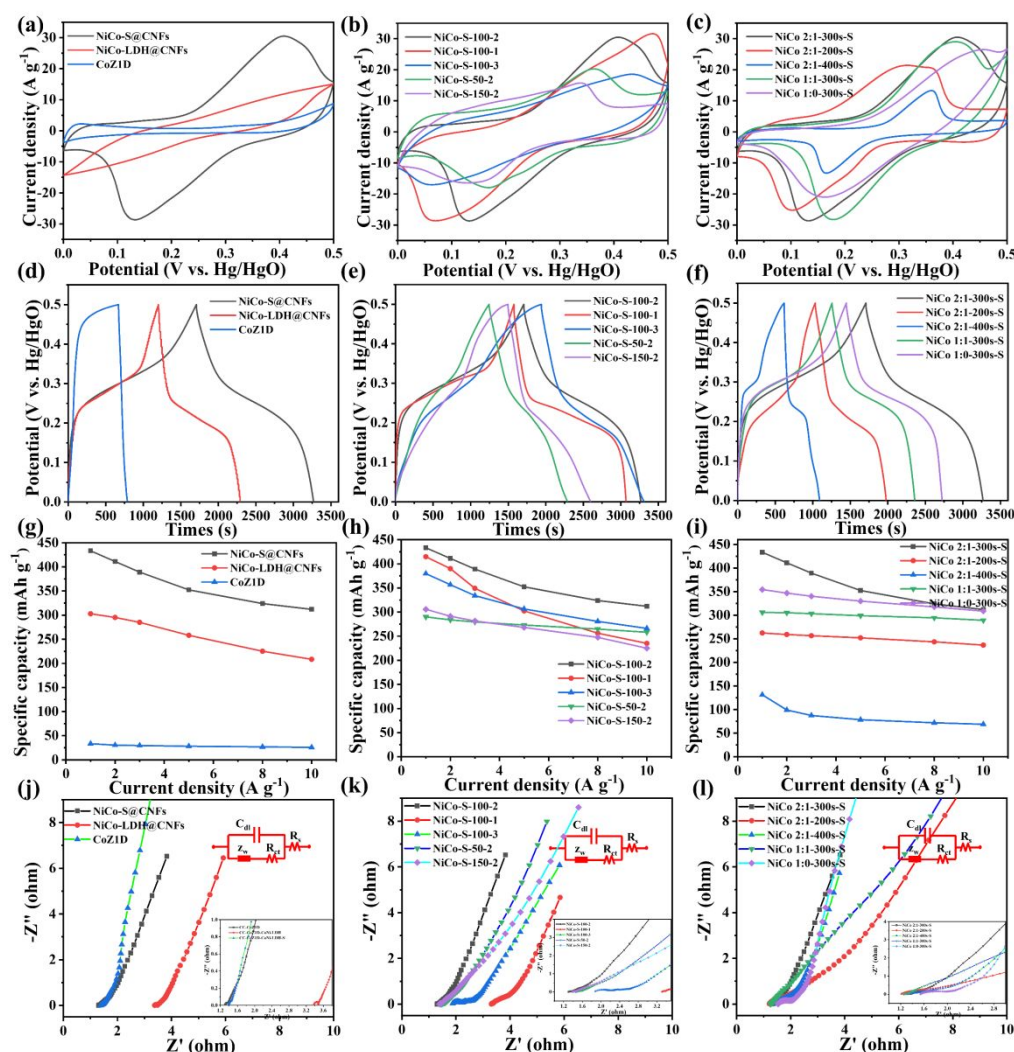


**Fig. 5.** Electrochemical performance comparison of samples with different steps (a, d, g, j), a concentration gradient of vulcanization (b, e, h, k), molar ratio regulation of metal (electrochemical deposition, c, f, i, l): CV at a scan rate of 2 mV s$^{-1}$ (a, b, c), GCD at a current density of 1 A g$^{-1}$ (d, e, f), rate capability at different current densities (1-10 A g$^{-1}$, g, h, i), and EIS curves (j, k, l).

The NiCo-S@CNFs electrode exhibits excellent specific capacity and stable cycling performance, which is mainly due to the construction of its superior hierarchical

20

structure with rich channels and synergistic active sites ($NiCo_2S_4$, $CoS_2$). Synthesis of

NiCo-LDH nanosheets on ZIF-L arrays, the hollow hierarchical structure increases the

contact area of the material with electrolyte, accelerates ion transport, and redox

processes, and provides abundant active sites after vulcanization, to further improve its

electrochemical performance. A model of the electron exchange transfer mode in the

electrolyte is shown in Fig. 6a. Moreover, the data of electrochemically active surface

area (ECSA) was tested, and its area gradually increased with the sulfurization of the

precursors, which is consistent with the electrochemical properties (Fig. 6b-c, Fig.

S6)[47]. Besides, the CV curves indicate the peak positions of redox in the electrode, as

the current density increases, the internal resistance will increase and the peak position

will move (Fig. 6d). To clarify its energy storage behavior, according to the formula:

$$i = a \cdot v^b \quad (3)$$

Among them, a and b are both constants, which are obtained by linearly processing the

peak currents of the oxidation/reduction peak positions at different current densities.

Generally speaking, the energy storage behavior is determined according to the

calculated b-value range. When the value of b is less than 0.5, it is mainly the diffusion-

controlled reaction; when the b value is greater than 1.0, it is a capacitive control; and

when it is in the range of 0.5-1.0, the mixed-type reaction (battery type) is controlled

for diffusion and capacitance. The b values obtained after processing the oxidation and

reduction peaks in the CV curve are 0.6282 and 0.6049, respectively. Therefore, the

values of b greater than 0.5 and less than 1.0, demonstrate that the energy storage

behavior is a mixed-type reaction and the electrode is a battery-type electrode (Fig. 6e).

21

The proportion of the pseudocapacitive contribution to the total energy storage capacity can be calculated according to the formula:

$$i\,(v) = k_1 \cdot v + k_2 \cdot v^{0.5} \quad (4)$$

Where $k_1$ and $k_2$ are constants calculated from the CV curves, and i and $v$ denote the current and the scan rate. Fig. S7 is the CV comparison diagrams of the pseudocapacitive contribution rate at different current densities (2, 3, 5, 8, and 10 mV $s^{-1}$), and the histogram of the pseudocapacitive proportion of the energy storage behavior at different current densities (Fig. 6f). The diffusion behavior of the NiCo-S@CNFs electrode accounts for a large proportion, so the electrode is mainly controlled by diffusion. The pseudocapacitance contribution rates are 18%, 19%, 21%, 27%, and 34%, and it is consistent with the energy storage properties of the active substance.
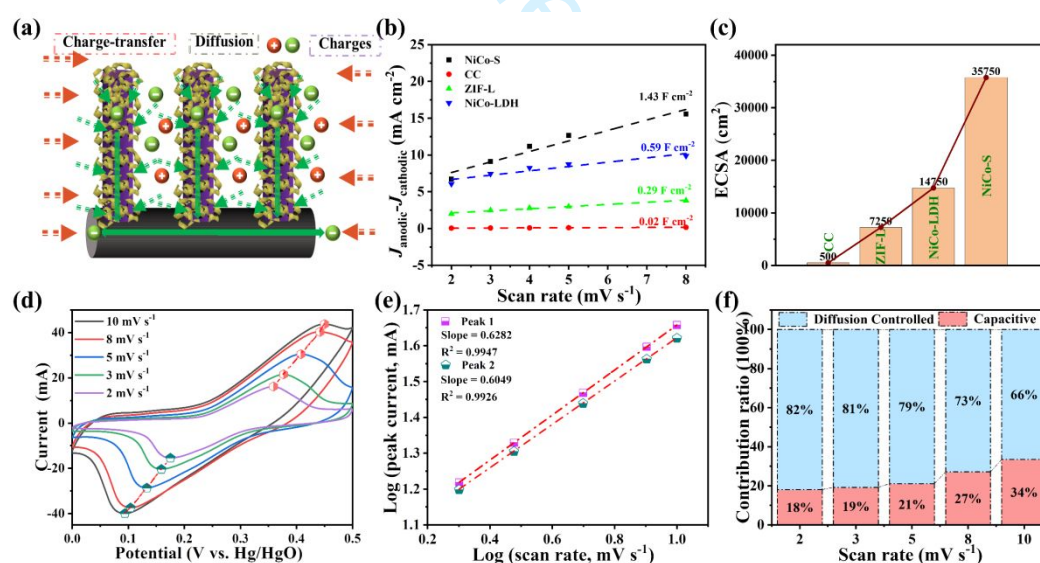


**Fig. 6.** The charge transport model of the multiphase active material NiCo-S@CNFs (a), current density difference in the non-Faraday region (0.1 V, 2-8 mV $s^{-1}$) (b) and the corresponding histogram of ECSA (c); the pseudocapacitance contribution diagram (d-f): CV curves with marked oxidation/reduction peaks (2-10 mV $s^{-1}$), the fitting linear regression curve, and the histogram.

22

The electrodes and AC were further assembled into HSC devices (NiCo-S@CNFs//AC), and their performance and stability were tested to estimate the worth of the electrodes for practical applications. Fig. 7a shows the CV curves of the positive and negative electrodes in a 6 M KOH environment system (2 mV s$^{-1}$). In a two-electrode system, the stored charge (specific capacity), voltage window, and mass of the two electrode materials need to be matched, according to the formula:

$$m_- = m_+ / ((C_- \times \Delta V_-) / C_+ \times \Delta V_+) \quad (5)$$

Among them, $C_m$ is the specific capacity (mAh g$^{-1}$), $\Delta V$ is the voltage window (V), m is the mass (g), and the mass of the anode material can be obtained. By changing the voltage window size of the two electrodes, the performance of the composed HSC was examined, and the CV and GCD curves at different voltages were obtained (Fig. 7b-c). In the range of 0-1.6 V (100 mV s$^{-1}$), the curve shape of both electrodes is well maintained, and a certain degree of polarization will occur when the potential exceeds 1.6 V, so the reasonable working voltage of the HSC device is 0-1.6 V. Similarly, the CV (2-100 mV s$^{-1}$) and GCD (1-10 A g$^{-1}$) curves of the HSC device were obtained by testing at the operating voltage of 0-1.6 V (Fig. 7d-e), and the specific capacitance was calculated (Fig. 7f). The specific capacitances at current densities of 1, 2, 3, 5, 8, and 10 mV s$^{-1}$ are 109, 101, 98.3, 94.6, 89.6, and 85.3 mAh g$^{-1}$, which display a great rate performance (78.3%, 1 to 10 A g$^{-1}$). In addition, the energy storage capacity of HSC devices can be determined by E (energy density, Wh kg$^{-1}$) and P (power density, W kg$^{-1}$), according to the formula[48]:

$$E = 0.5 \times (C \times \Delta V^2) / 3.6 \quad (6-1)$$

$$P = (E \times 3600) / \Delta t \qquad (6\text{-}2)$$

where C, V, and t are the specific capacity (F $g^{-1}$), the potential (V), and the discharge time (s). According to the calculation, when the power density is 800 W $kg^{-1}$, the maximum energy density of the electrode is 87.2 Wh $kg^{-1}$. Besides, the high energy density of HSCs devices at large power densities is demonstrated by Ragone plots, and the energy density of NiCo-S@CNFs//AC and other previously reported HSCs are compared (Fig. 7g, Table 1).

**Table 1.** Data of recent works in the Ragone graph.

| Supercapacitor | Energy density (Wh $kg^{-1}$) | Power density (W $kg^{-1}$) | Reference |
|---|---|---|---|
| CNZ-CH NRAs@NF//FEG | 68.3 | 65.1 | [23] |
| NiCo$_2$S$_4$//rGO/Fe$_2$O$_3$ | 61.7 | 1200 | [49] |
| NiCoP@CoS//AC | 53.8 | 853 | [50] |
| HC-NCS@MXene//AC-AHSC | 80 | 1196 | [51] |
| NiCoMn-S//AC | 50 | 850 | [52] |
| NiCo-P//PANI/rGO | 43.4 | 620 | [53] |
| Ni/Co-N-350//AC | 20.4 | 985 | [54] |
| Co-OH/G//AC | 45.1 | 800 | [55] |
| NiCo-S@CNFs//AC | 87.2 | 800 | This work |

The EIS of the device is shown in Fig. 7h. Cycling stability tests were performed on the composed HSC devices in 6 M KOH electrolytes (Fig. 7i). There is a certain increase in capacity during the first 4000 cycles, which is because the electrode has continuous contact and is in the process of continuous activation. After 6000 cycles, the capacity of the HSC device increased to 109.1 % of the original, indicating that it has good stability and tends to be stable. In the following 6000-12000 cycles, the

24

measured capacity stability fluctuated slightly, which was due to the temperature difference between day and night and the capacitance fluctuation caused by the volatilization of the electrolyte during the long-term test. Overall, the HSC has a relatively stable capacity with 105.1% capacity retention after 12,000 cycles and still maintains a good hollow hierarchical structure after testing (Fig. S8). It was also tested for three-electrode cycle stabilities (5 A g$^{-1}$) and had 91.1% capacity retention after 2000 charge/discharge reactions (Fig. S9), indicating its structure is stable and has great value for application in the energy storage/conversion industry.
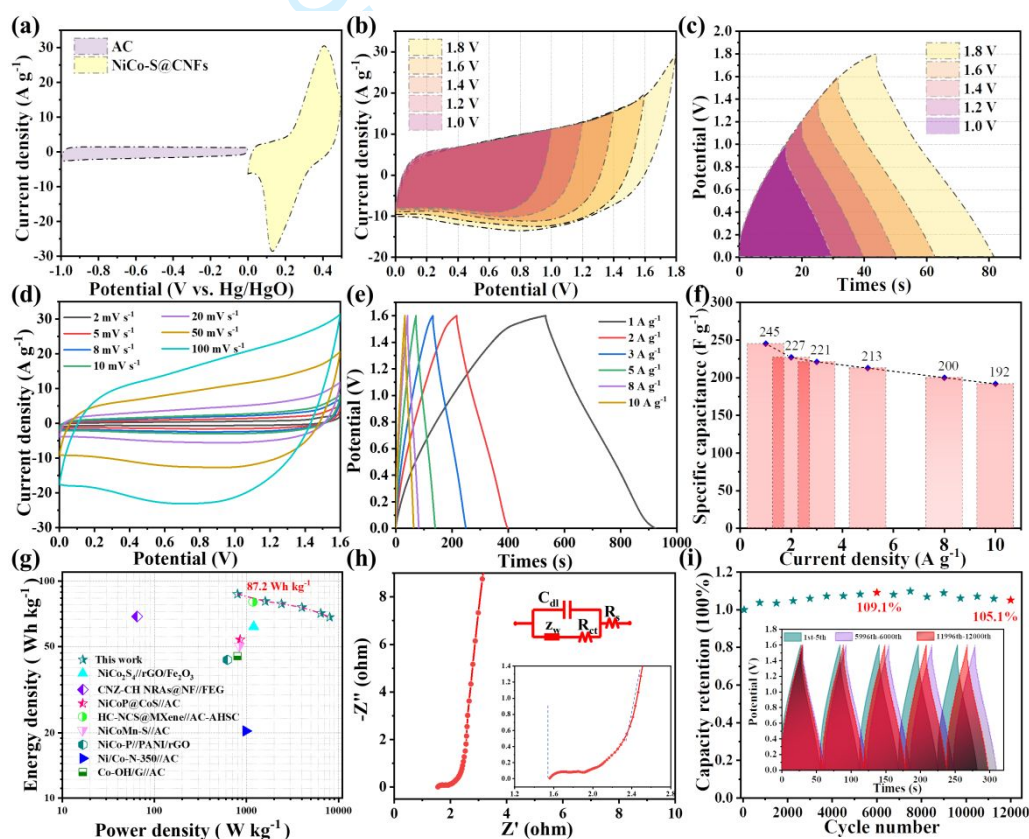


**Fig. 7.** (a) CV curves at 2 mV s$^{-1}$ of the two electrode NiCo-S@CNFs and AC; (b-c) CV comparison at 100 mV s$^{-1}$ and GCD curves at 10 A g$^{-1}$ (1.0-1.8 V), (d-e) CV and GCD curve in detailed, (f-h) rate performance graph, Ragone graph, EIS curve, (i) 12,000 cycle stability test graph of the HSC (NiCo-S@CNFs//AC).

The charge and discharge model (HSC: NiCo-S@CNFs//AC) is shown in Fig. 8a, revealing the direction and path of electron transport in the energy storage reaction. To estimate the practical value of the electrodes, two assembled HSC devices were attached in series to form a complete circuit with paralleled LED lamps (Fig. 8b-d). The rated voltage of the device is 3.2 V, and the LED lamp can be successfully turned on after a short charge, which demonstrates that it has great practical value and potential.
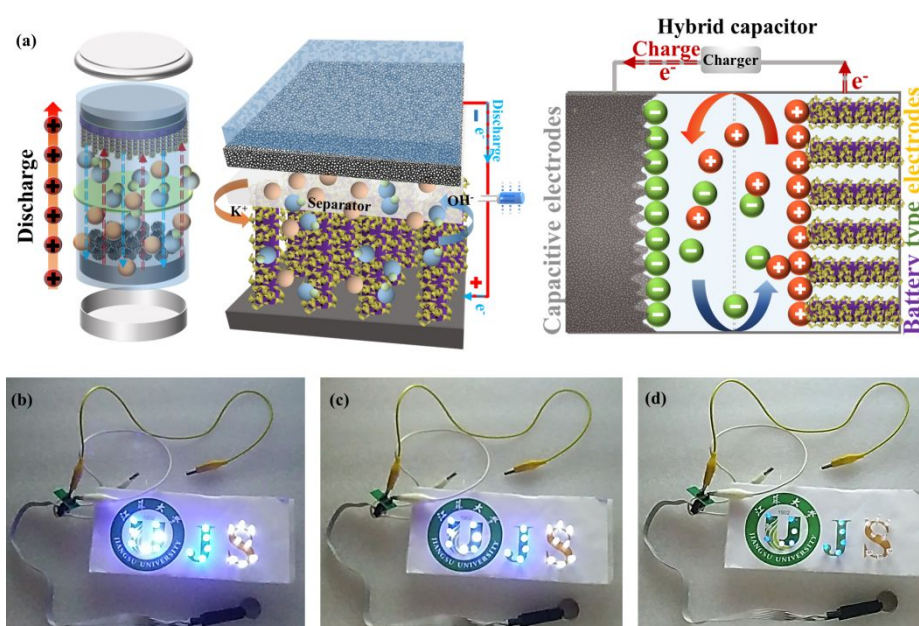


**Fig. 8.** (a) Charge transfer model in charge and discharge; (b-d) multiple LEDs are lit with HSCs.

## 4. Conclusion

In sum, the reasonable hierarchical multiphase composite NiCo-S@CNFs/CC ($NiCo_2S_4$, $CoS_2$) was successfully prepared. Modification of ZIF-L with an electrochemical strategy is the key to forming hollow hierarchical structures and enriching the redox reactions by introducing metal ions. The above strategy protects the original structure from being destroyed, promotes the electron transfer rate, and provides a superior platform for the synthesis of the multiphase materials. Then, by forming different metal sulfides through sulfidation, the multiphase synergy further

26

enhances the redox activity and promotes the capacity and stability of the active electrode. The results show that the strategy is feasible and the prepared multiphase inhomogeneous structured electrodes have good electrochemical performance and stability. It was assembled with AC to form a hybrid supercapacitor (HSC, NiCo-S@CNFs/CC//AC) with high energy density and good cycling stability, and it can light up LED lamps. Therefore, the construction of complex fine structures and synthesis of electrodes with synergistic multiphase active materials are the keys to obtaining good electrochemical performance and stability with great potential and application prospects.

**CRediT authorship contribution statement**

**Lin Sun:** Conceptualization, Data curation, Formal analysis, Supervision, Validation, Visualization, Writing - review & editing, Funding acquisition. **Fangrong Yan:** Investigation, Methodology, Project administration. **Chunxiao Shi:** Validation, Visualization. **Hang Wei:** Validation, Visualization. **Yu Liu:** Investigation. **Qingjun Yang:** Investigation. **Runmei Luo:** Investigation. **Guiquan Liu:** Investigation. **Weidong Shi:** Funding acquisition, Data curation, Supervision, Methodology, Project administration.

**Declaration of Competing Interest**

The authors declare that they have no known competing financial interests or personal relationships that could have appeared to influence the work reported in this paper.

**Acknowledgments**

## 5. References

[1] KH. Wang, X. Gao, Y. Xie, E. Guo, H. Bai, F. Jiang, Q. Li, H. Yue, *Advanced Energy Materials* **2024**, 14, 32, 2400493.

[2] H. Hu, C. Yang, F. Chen, J. Li, X. Jia, Y. Wang, X. Zhu, Z. Man, G. Wu, W. Chen, *Advanced Materials* **2024**, 36, 35, 2406483.

[3] Y. Ai, C. Yang, Z. Yin, T. Wang, T. Gai, J. Feng, K. Li, W. Zhang, Y. Li, F. Wang, D. Chao, Y. Wang, D. Zhao, W. Li, *Journal of the American Chemical Society* **2024,** 146, 22, 15496-15505

[4] H. Chen, T. Liu, J. Mou, W. Zhang, Z. Jiang, J. Liu, J. Huang, M. Liu, *Nano Energy* **2019**, 63.

[5] Q. Yang, Q. Wang, Y. Long, F. Wang, L. Wu, J. Pan, J. Han, Y. Lei, W. Shi, S.

Song, *Advanced Energy Materials* **2020**, 10, 7.

[6] K. Li, Z. Guo, Q. Sun, X. Dai, Y. Li, K. Yao, X. Liu, Z. Bao, J. Rao, Y. Zhang, *Chemical Engineering Journal* **2023**, 454, 140223.

[7] T. Wang, H.C. Chen, F. Yu, X.S. Zhao, H. Wang, *Energy Storage Materials* **2019**, 16, 545-573.

[8] Q. Yang, K. Y. Chung, X. Liu, L. Sun, J. Han, Y. Yang, T. Chen, W. Shi, B. Xu, *Advanced Materials* **2024**, 2401375.

[9] W. Ye, P. Ye, H. Wang, F. Chen, Y. Zhong, Y. Hu, *Journal of Colloid and Interface Science* **2022**, 612, 298-307.

[10] H. Wang, Y. Yang, Q. Li, W. Lu, J. Ning, Y. Zhong, Z. Zhang, Y. Hu, *Science China Materials* **2021**, 64, 840-851.

[11] Y. Wen, S. Peng, Z. Wang, J. Hao, T. Qin, S. Lu, J. Zhang, D. He, X. Fan, G. Cao, *Journal of Materials Chemistry A* **2017**, 5, 15, 7144-7152.

[12] T.-F. Yi, J.-J. Pan, T.-T. Wei, Y. Li, G. Cao, *Nano Today* **2020**, 33.

[13] M. Liang, M. Zhao, H. Wang, J. Shen, X. Song, *Journal of Materials Chemistry A* **2018**, 6, 6, 2482-2493.

[14] F. Yu, Z. Chang, X. Yuan, F. Wang, Y. Zhu, L. Fu, Y. Chen, H. Wang, Y. Wu, W. Li, *Journal of Materials Chemistry A* **2018**, 6, 14, 5856-5861.

[15] X. Lei, Y. Zhang, J. Han, X. Su, L. Xue, W. Guo, Y. Zhang, *Chemical Engineering Journal* **2024**, 152728.

[16] Y. Li, X. Wei, F. Jiang, Y. Wang, M. Xie, J. Peng, C. Yi, J. Li, M. Zhai, *Energy & Environmental Materials* **2024**, e12820.

[17] L. Sun, Y. Liu, B. Luo, F. Yan, X. Liu, F. Zhu, W. Shi, *Chemical Engineering Journal* **2023**, 454.

[18] Y. Cui, J. Zhang, C. Jin, Y. Liu, W. Luo, W. Zheng, *Small* **2018**, 15, 3.

[19] K. Li, C. Yin, X. Dai, J. Zhang, S. Yi, J. Rao, Y. Zhang, *Journal of Energy Storage* **2022**, 55, 105722.

[20] C. Zhang, K. Li, T. Sun, X. Liu, X. Dai, Q. Zhou, D. Wang, X. Zhang, J. Ding, X. Huang, J. Rao, Y. Hou, P. Yang, K. Liu, Y. Zhang, *ACS Applied Nano Materials* **2024**, 7, 3001-3011.

[21] Q. Li, W. Lu, Z. Li, J. Ning, Y. Zhong, Y. Hu, *Chemical Engineering Journal* **2020**, 380.

[22] X. Yin, C. Zhi, W. Sun, L.-P. Lv, Y. Wang, *Journal of Materials Chemistry A* **2019**, 7, 13, 7800-7814.

[23] F. Sun, C. Wu, X. Guan, Z. Huang, X. Han, Y. Zhang, H. Li, Y. Song, T. Ma, *Advanced Functional Materials* **2024**, 2415255.

[24] X. Wang, F. Huang, F. Rong, P. He, R. Que, S.P. Jiang, *Journal of Materials Chemistry A* **2019**, 7, 19,12018-12028.

[25] L. Sun, Y. Liu, M. Yan, Q. Yang, X. Liu, W. Shi, *Chemical Engineering Journal* **2022**, 431.

[26] W. Liu, Y. Zhao, J. Zheng, D. Jin, Y. Wang, J. Lian, S. Yang, G. Li, Y. Bu, F. Qiao, *Journal of Colloid and Interface Science* **2022**, 606, 728-735.

[27] L. Sun, Y. Liu, Q. Yang, Fangrong Yan, X. Liu, C. Wang, R. Luo, W. Shi, *Chemical Engineering Science* **2023**, 278: 118905.

30

Materials Lab

[28] G. Qu, C. Li, P. Hou, G. Zhao, X. Wang, X. Zhang, X. Xu, *Nanoscale* **2020**, 12, 7, 4686-4694.

[29] S.L. Zhang, B.Y. Guan, X.F. Lu, S. Xi, Y. Du, X.W. Lou, *Advanced Materials* **2020**, 32, 31.

[30] Y. Feng, X. Wang, J. Huang, P. Dong, J. Ji, J. Li, L. Cao, L. Feng, P. Jin, C. Wang, *Chemical Engineering Journal* **2020**, 390.

[31] H. Li, Y. Su, W. Sun, Y. Wang, Carbon Nanotubes Rooted in Porous Ternary *Advanced Functional Materials* **2016**, 26, 45, 8345-8353.

[32] F. Yuan, J. Wei, G. Qin, Y. Ni, *Journal of Alloys and Compounds* **2020**, 830.

[33] Y. Zhu, S. An, X. Sun, D. Lan, J. Cui, Y. Zhang, W. He, *Chemical Engineering Journal* **2020**, 383.

[34] J. Huang, S. Wang, J. Nie, C. Huang, X. Zhang, B. Wang, J. Tang, C. Du, Z. Liu, J. Chen, *Chemical Engineering Journal* **2021**, 417.

[35] Y. Li, B. Zhang, W. Wang, X. Shi, J. Zhang, R. Wang, B. He, Q. Wang, J. Jiang, Y. Gong, H. Wang, *Chemical Engineering Journal* **2021**, 405.

[36] K. A. Nirmal, W. Ren, A. C. Khot, D. Y. Kang, T. D. Dongale, T. G. Kim, *Advanced Science* **2023**, 10, 19, 2300433.

[37] X. Wang, T. Song, G. Fu, Y. Yang, *ACS Catalysis* **2023**, 13, 17, 11634-11643.

[33] Q. Cheng, Z. Chen, X. Li, C. Bi, F. Sun, X. Zhang, X. Ma, B. Li, J. Huang, *Advanced Energy Materials* **2023**, 13, 42, 2301770.

[38] Q. Cheng, Z. Chen, X. Li, C. Bi, F. Sun, X. Zhang, X. Ma, B. Li, J. Huang, *Advanced Energy Materials* **2023**, 13, 42, 2301770.

31

[39] P. Lv, S. Chang, Q. Hong, J. Mei, S. Yang, *Chemical Engineering Journal* **2024**, 483: 148955.

[40] J. Gao, Y. Hu, Y. Wang, X. Lin, K. Hu, X. Lin, G. Xie, X. Liu, K.M. Reddy, Q. Yuan, H.J. Qiu, *Small* **2021**, 17, 49.

[41] Y. Fu, H.Y. Yu, C. Jiang, T.H. Zhang, R. Zhan, X. Li, J.F. Li, J.H. Tian, R. Yang, *Advanced Functional Materials* **2017**, 28, 9.

[42] X. Yin, Y. Ren, S. Guo, B. Sun, L. Wu, C. Du, J. Wang, G. Yin, H. Huo, *Advanced Functional Materials* **2022**, 32, 22.

[43] W. Chen, X. Zhang, L.-E. Mo, Y. Zhang, S. Chen, X. Zhang, L. Hu, *Chemical Engineering Journal* **2020**, 388.

[44] J. Pu, F. Cui, S. Chu, T. Wang, E. Sheng, Z. Wang, *ACS Sustainable Chemistry & Engineering* **2018**, 2, 4, 809-815.

[45] M. Yan, Y. Yao, J. Wen, L. Long, M. Kong, G. Zhang, X. Liao, G. Yin, Z. Huang, *ACS Applied Materials & Interfaces* **2016**, 8, 37, 24525-24535.

[46] L. Mei, T. Yang, C. Xu, M. Zhang, L. Chen, Q. Li, T. Wang., *Nano Energy* 2014, 3, 36-45.

[47] M. Gao, K. Le, G. Wang, Z. Wang, F. Wang, W. Liu, J. Liu, *Electrochimica Acta* **2019**, 323.

[48] J. Zhang, J. Luo, Z. Guo, Z. Liu, C. Duan, S. Dou, Q. Yuan, P. Liu, K. Ji, C. Zeng, J. Xu, W. Liu, Y. Chen, W. Hu, *Advanced Energy Materials* **2023**, 13, 1, 2203061.

[49] Y. Wang, Z. Chen, T. Lei, Y. Ai, Z. Peng, X. Yan, H. Li, J. Zhang, Z.M. Wang, Y.L. Chueh, *Advanced Energy Materials* **2018**, 8, 16.

32

[50] Z. Xu, C. Du, H. Yang, J. Huang, X. Zhang, J. Chen, *Chemical Engineering Journal* **2021**, 421.

[51] W. Yang, C. Zhang, B. Jiang, P. Wang, L. Yan, L. Hou, F. Yang, Y. Li, *Chemical Engineering Journal* **2022**, 434: 134473.

[52] C. Kang, L. Ma, Y. Chen, L. Fu, Q. Hu, C. Zhou, Q. Liu, *Chemical Engineering Journal* **2022**, 427, 131003.

[53] Z. Liang, C. Qu, W. Zhou, R. Zhao, H. Zhang, B. Zhu, W. Guo, W. Meng, Y. Wu, W. Aftab, Q. Wang, R. Zou, *Advanced Science* **2019**, 6.

[54] X. Liu, W. Zang, C. Guan, L. Zhang, Y. Qian, A.M. Elshahawy, D. Zhao, S.J. Pennycook, J. Wang, *ACS Energy Letters* **2018**, 3, 2462-2469.

[55] M. S. Javed, X. Zhang, S. Ali, A. Mateen, M. Idrees, M. Sajjad, S. Batool, A. Ahmad, M. Imran, T. Najam, W. Han, *Nano Energy* **2022**, 101, 107624.

**Reviewer: 1**

Comments to the Author

This manuscript presents Electrochemical rapid reconstruction of 1D ZIF-L derived hollow hierarchical multiphase NiCo-S for high-performance hybrid supercapacitors. I suggest a major revision. I think the manuscript can be reconsidered for the next step after addressing some comments:

1. In this manuscript, there are some mistakes in your manuscript. Please correct them marked in yellow and polish your language carefully.

**Response:**

Thanks very much for your suggestion. We must apologize for some typos and grammatical and descriptive errors that we have not been cautious about enough. After careful inspection, we have solved some of them, hoping to improve the rigor and fluency of the manuscript and avoid causing trouble to the reviewers. The corrected part has been marked in yellow and red in the manuscript and supplementary materials.

2. The abstract should be to the point giving the context of the entire research work carried out.

**Response:**

Thanks very much for your suggestion. We strongly agree that the summary of your suggestion should be to the point and give context to the overall research work undertaken. We have made some changes, specifically as follows:

**Abstract**

The combination of low electronegative sulfur and common transition metals has obvious advantages in easing volume expansion and improving electrical conductivity for energy storage. Herein, we developed an electrochemically assisted strategy to rapidly reconstruct ZIFs (Zeolitic Imidazolate Frameworks) with Lewis acid to obtain reticulated cross-linked hierarchical electrode NiCo-LDH@CNFs (carbon-nitrogen frameworks) with excellent active specific surface area. Simple vulcanization can effectively optimize the active site and crystal structure, and further improve the conductivity of the multi-phase electrode NiCo-S@CNFs ($NiCo_2S_4$, $CoS_2$). Furthermore, the synergistic effect of multi-phase metal sulfides and the reasonable structure can effectually enhance the redox activity, adsorption capacity of $OH^-$, and reduce the volume expansion and of the electrode. The results demonstrate that the specific capacity of the electrode is 433.3 mAh $g^{-1}$ (6 M KOH). The prepared HSC device (hybrid supercapacitor, NiCo-S/CNFs//AC (activated carbon)) exhibits a maximum energy density of 87.2 Wh $kg^{-1}$ (800 W $kg^{-1}$). After 12,000 charge/discharge cycles, the capacity retention rate is still 105.1%, which has excellent cycling stability among ZIF-derived binary metal sulfides. Furthermore, parallel-connected LEDs can be lit by two series-connected HSCs, showing their practicality and great potential.

3. Authors must justify the differences in comparison with the other reported review papers.

**Response:**

Thanks very much for your suggestion. We summarize the differences between our work and others as follows:

**1.** We developed an electrochemically assisted strategy to rapidly reconstruct ZIFs (Zeolitic Imidazolate Frameworks) with Lewis acid to obtain reticulated cross-linked hierarchical electrode NiCo-LDH@CNFs (carbon-nitrogen frameworks) with excellent active specific surface area. The simple and effective reconstruction strategy is superior to similar work in terms of stability, conductivity increase, and active specific surface area increase.

**2.** The reasonable hierarchical structure effectively reduces the volume expansion phenomenon and electrochemically modifies the ZIF-L efficiently, while the internal composition and structure remain unchanged due to its unique structure, forming a graded structure with different internal and external components.    The multi-phase active material then further reduces the internal resistance, increases the conductivity of the electrode, and effectively improves its electrochemical performance and cycling stability. This work provides ideas for the efficient integration of building hierarchical structures and heterogeneous multiphase systems with enhanced stability.

**3.** Compared with some previous works, the high-performance electrode NiCo-S@CNFs in this work demonstrate superior capacity and stability, as shown in **Table S1**. In addition, when assembled into HSC (NiCo-S@CNFs/CC//AC), it also exhibits excellent capacity, energy density, and long-cycle stability, as shown in **Table 1**.

Therefore, the electrodes in this work are different from those previously reported in many aspects, including design synthesis strategy, energy storage mechanism, electrochemical performance, and stability.

**Table S1.** Electrochemical performance comparisons between this work and previous reports**.**

| Materials | Electrolyte | Capacity (Three-electrode system) | Capacity (Two-electrode system) | Retention (Two-electrode system) | Ref |
|---|---|---|---|---|---|
| $NiCo_2S_4$ | 4 M KOH+1 M LiOH | 254.7 mAh g$^{-1}$ (1.0 A g$^{-1}$) | 63.2 mAh g$^{-1}$ (1.0 A g$^{-1}$) | 91.0% after 3,500 cycles | [S2] |
| Porous $NiCo_2S_4$ | 6 M KOH | 223.6 mAh g$^{-1}$ (1.0 A g$^{-1}$) | 65 mAh g$^{-1}$ (1.0 A g$^{-1}$) | 95.3% after 6,000 cycles | [S3] |
| NiCoP@CoS | 3 M KOH | 249.4 mAh g$^{-1}$ (2.0 A g$^{-1}$) | 47.8 mAh g$^{-1}$ (1.0 A g$^{-1}$) | 91.6% after 10000 cycles | [S4] |
| $Zn_{0.76}Co_{0.24}S@Ni_3S_2$ | 6 M KOH | 335.8 mAh g$^{-1}$ (2.0 A g$^{-1}$) | 63.3 mAh g$^{-1}$ (1.0 A g$^{-1}$) | 87.5% after 20,000 cycles | [S5] |
| CS NTs@Ni-Co LDH NSs | 6 M KOH | 283.3 mAh g$^{-1}$ (0.5 A g$^{-1}$) | 65.6 mAh g$^{-1}$ (1.0 A g$^{-1}$) | 85.2% after 3,000 cycles | [S6] |
| NiCo-P | 2 M KOH | 248.3 mAh g$^{-1}$ (0.5 A g$^{-1}$) | / | 90.2% after 10,000 cycles | [S7] |
| Ni/Co-N-350 | 1 M KOH | 100.5 mAh g$^{-1}$ (2.0 mA cm$^2$) | 25.9 mAh g$^{-1}$ (2.0 mA cm$^2$) | 88.0% after 5,000 cycles | [S8] |
| H-NiCoSe$_2$ | 6 M KOH | 83.3 mAh g$^{-1}$ (3.0 A g$^{-1}$) | 106.7 mAh g$^{-1}$ (3.0 A g$^{-1}$) | 98.0% after 12,000 cycles | [S9] |
| HMFO-CSN | 6 M KOH | 248.3 mAh g$^{-1}$ (1.0 A g$^{-1}$) | 75.0 mAh g$^{-1}$ (1.0 A g$^{-1}$) | 90.5% after 10,000 cycles | [S10] |
| MnO$_2$@NiCo-LDH/CoS$_2$ | 2 M KOH | 236.3 mAh g$^{-1}$ (1.0 A g$^{-1}$) | 64.3 mAh g$^{-1}$ (0.5 A g$^{-1}$) | 81.0% after 2,000 cycles | [S11] |
| NiCo-S/CNFs | 6 M KOH | 424.7 mAh g$^{-1}$ (1.0 A g$^{-1}$) | 108.9 mAh g$^{-1}$ (1 A g$^{-1}$) | 105.1% after 12,000 cycles | This work |

**Table 1.** Data of recent works in the Ragone graph.

| Supercapacitor | Energy density (Wh kg$^{-1}$) | Power density (W kg$^{-1}$) | Reference |
|---|---|---|---|
| CNZ-CH NRAs@NF//FEG | 68.3 | 65.1 | [23] |
| NiCo$_2$S$_4$//rGO/Fe$_2$O$_3$ | 61.7 | 1200 | [49] |
| NiCoP@CoS//AC | 53.8 | 853 | [50] |
| HC-NCS@MXene//AC-AHSC | 80 | 1196 | [51] |
| NiCoMn-S//AC | 50 | 850 | [52] |
| NiCo-P//PANI/rGO | 43.4 | 620 | [53] |
| Ni/Co-N-350//AC | 20.4 | 985 | [54] |
| Co-OH/G//AC | 45.1 | 800 | [55] |
| NiCo-S@CNFs//AC | 87.2 | 800 | This work |

4. The background of this paper should be enhanced by citing all the following references, such as J. Am. Chem. Soc. 2024, 146, 22, 15496–15505 Chemical Engineering Journal 454 (2023) 140223; Journal of Energy Storage 55 (2022) 105722; ACS Appl. Nano Mater. 2024, 7, 3, 3001–3011.

**Response:**

Thank you very much for your suggestion. We agree that some recent related works should be cited and discussed appropriately. The references will provide us with better guidance in the fields of supercapacitors, design strategies, and further energy storage mechanisms of high-performance electrodes. In addition, the supplement of relevant references makes our manuscript perfect. We have added them to the manuscript for theoretical support. Thank you again for your suggestion.

**Reviewer: 2**

Comments to the Author

The authors have conducted extensive and systematic research on the high-performance electrodes (hollow hierarchical multi-phase NiCo-S@CNFs) for hybrid-supercapacitor. The electrode design has a certain novelty. The adequate characterization and performance testing can fully demonstrate the superiority and application prospects of the electrode. I suggest the manuscript can be published after addressing few comments given below:

1. The author should explain how to reconstruct the precursor using electrochemical methods and explain its mechanism of action.

**Response:**

Thanks very much for your suggestion. We agree that it is necessary to explain how to reconstruct the precursor electrochemically and explain its mechanism of action. Specifically, when the traditional Lewis acid reconstructed ZIFs are used to prepare high-performance electrodes:

**1.** when the concentration of Lewis acid is small, it takes a long time (several hours or tens of hours) to fully realize the etching/exchange of metal ions on ZIFs, and the limited number of metal active sites also limits the energy storage capacity of the electrode;

**2.** when the concentration of Lewis acid is large, although the etching/exchange time is greatly shortened (tens of minutes), the energy storage capacity of the electrode is

increased but limited, and the collapsibility structure is not conducive to the electrochemical stability of the electrode;

**3.** With the assistance of the chronoamperometry method (i-t), the etching/exchange of metal ions on ZIFs can be completed within a few minutes under the condition of a large concentration of Lewis acid, and the maximum amount of active sites per unit area can be achieved while the formation of the cross-linked multistage structure of highly stable nanosheets can be achieved, and the energy storage capacity and stability can be realized.

Furthermore, with the help of the chronoamperometry method, the three-electrode system forms a current loop, and the positively charged metal ions (Ni, Co) accelerate to move to the working electrode (precursor material ZIFs). At the same time, a large amount of $OH^-$ is generated around the working electrode due to the reaction of electrons and water. A highly stable multistage hollow NiCo-LDH@CNFs (carbon and nitrogen skeleton) cross-linked with nanosheets was formed on 1D ZIFs, while a large number of metal active sites were exposed on the surface of the nanosheets, laying a foundation for further vulcanization and further improvement of electronic structure, active sites, surface small area, capacity, and stability.

2. Throughout the paper, there is no mention of active material(s) loading mass(es) for the prepared electrode(s).

**Response:**

Thanks very much for your suggestion. We are sorry that we are missing the description

of active materials loading masses. It is well known that the loading masses of active materials on the substrate (collector, CC) are the determining factor (calculation formula) of the electrochemical performance of the electrodes. In the experimental section of the manuscript, we have supplemented the loading masses on the active substances after weighing. Specific loading masses of active substances in different steps are as follows: **Section 2.1**, The loading mass of precursor ZIF-L nanoarrays on CC was 1.5 mg cm$^{-2}$. **Section 2.2**, The loading mass of intermediate NiCo-LDH@CNFs on CC was 2.0-2.5 mg cm$^{-2}$. The mass of the intermediate is slightly increased due to the different degrees of in-situ reconstruction. **Section 2.3**, The loading mass of active substance NiCo-S/CNFs on CC was 2.5-3.0 mg cm$^{-2}$. The depth of vulcanization leads to the generation of new phases (multiphase polyphase sulfides) with a certain increase in loading mass. Thanks again for your suggestion. The revised content has been marked yellow and red in the manuscript (Section 2.1-2.3).
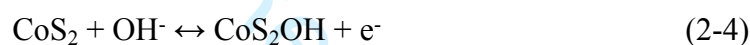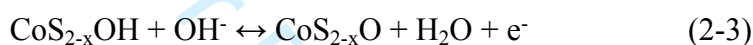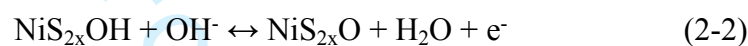
3. It is imperative to conduct characteristic analysis of the samples post-durability testing, with corresponding data and descriptions provided by the authors.

**Response:**

Thanks very much for your suggestion. We strongly agree that the characterization of the electrode after the durability test is of great importance to the analysis of the energy storage mechanism of the electrode. Therefore, we further analyzed our existing physical characterization and data, supplemented the electrode element mapping and EDS spectrum after the durability test, consulted more literature, and further analyzed

the reaction mechanism in this work. Relevant contents have been supplemented in the manuscript and supplementary materials, and the specific modifications are as follows:

**1.** We continue to consult the literature to further confirm, supplement, and correct the redox reaction of polyphase electrode materials in alkaline electrolyte KOH, and relevant contents have been supplemented and corrected in the manuscript, specifically as follows:

$$NiCo_2S_4 + 2OH^- \leftrightarrow NiS_{2x}OH + 2CoS_{2-x}OH + 2e^- \qquad (2-1)$$

$$NiS_{2x}OH + OH^- \leftrightarrow NiS_{2x}O + H_2O + e^- \qquad (2-2)$$

$$CoS_{2-x}OH + OH^- \leftrightarrow CoS_{2-x}O + H_2O + e^- \qquad (2-3)$$

$$CoS_2 + OH^- \leftrightarrow CoS_2OH + e^- \qquad (2-4)$$

$$CoS_2OH + OH^- \leftrightarrow CoS_2O + H_2O + e^- \qquad (2-5)$$

**2.** We carried out element mapping and EDS spectrum characterization on the electrodes after the durability test (Fig. S2-4). First of all, the element mapping showed that the elements (C, N, O, Ni, Co, S) of the sample NiCo-S@CNFs still existed and dispersed uniformly after the durability test. Therefore, there is a certain amount of K, and the corresponding elements have obvious characteristic peaks in the EDS spectra, which is consistent with the fact, indicating that the original phase sulfide still exists after the durability test. Compared with the samples before the endurance test, the O content increased significantly and the S content decreased correspondingly, which was consistent with the fact that the intermediates NiS-O and CoS-O were produced during the electrochemical redox process in the literature.
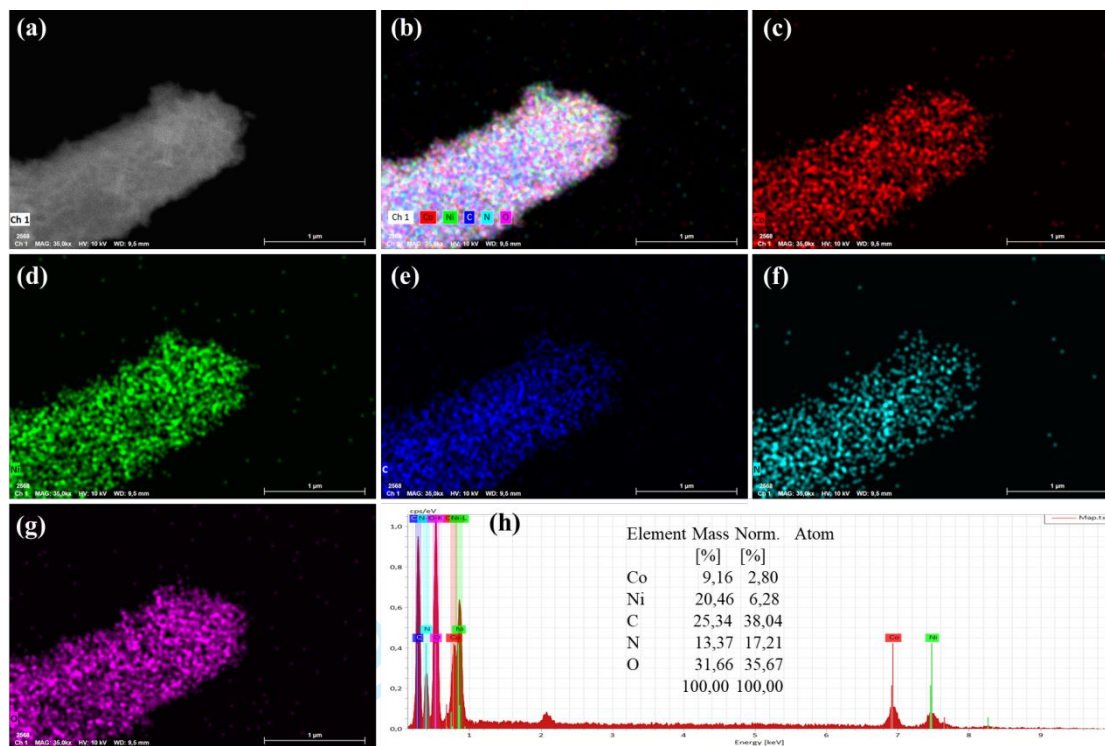
**Fig. S2-1.** FESEM element mapping and energy spectrum of the intermediate NiCo-LDH@CNFs.
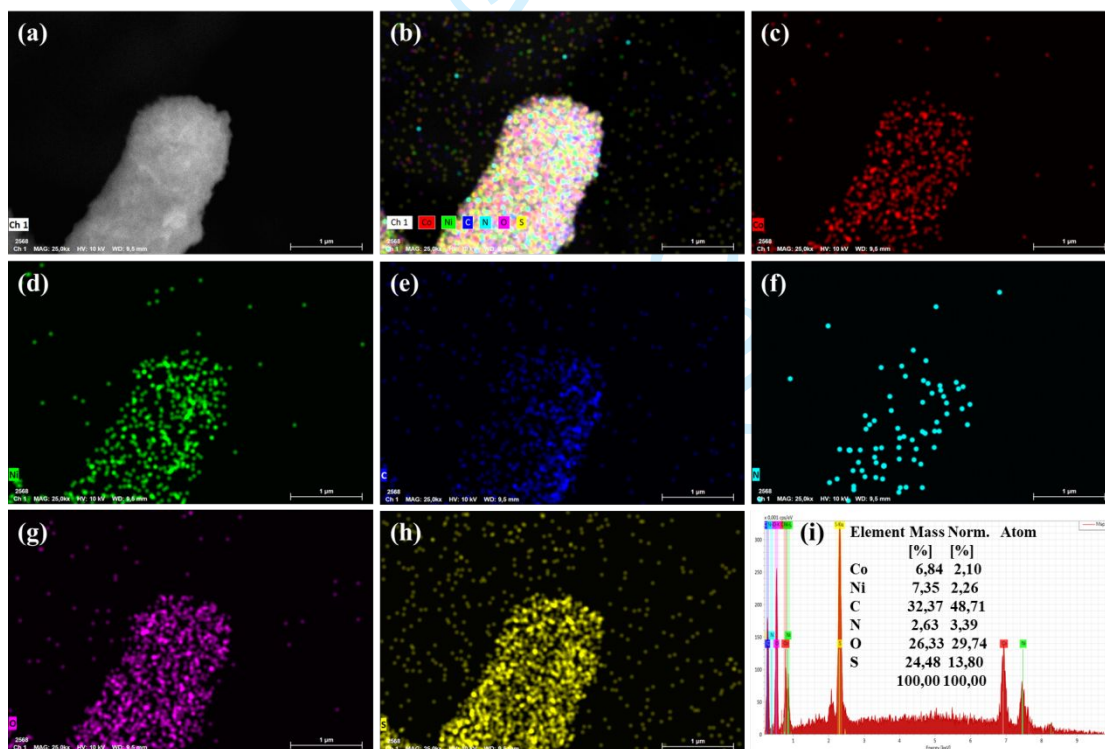


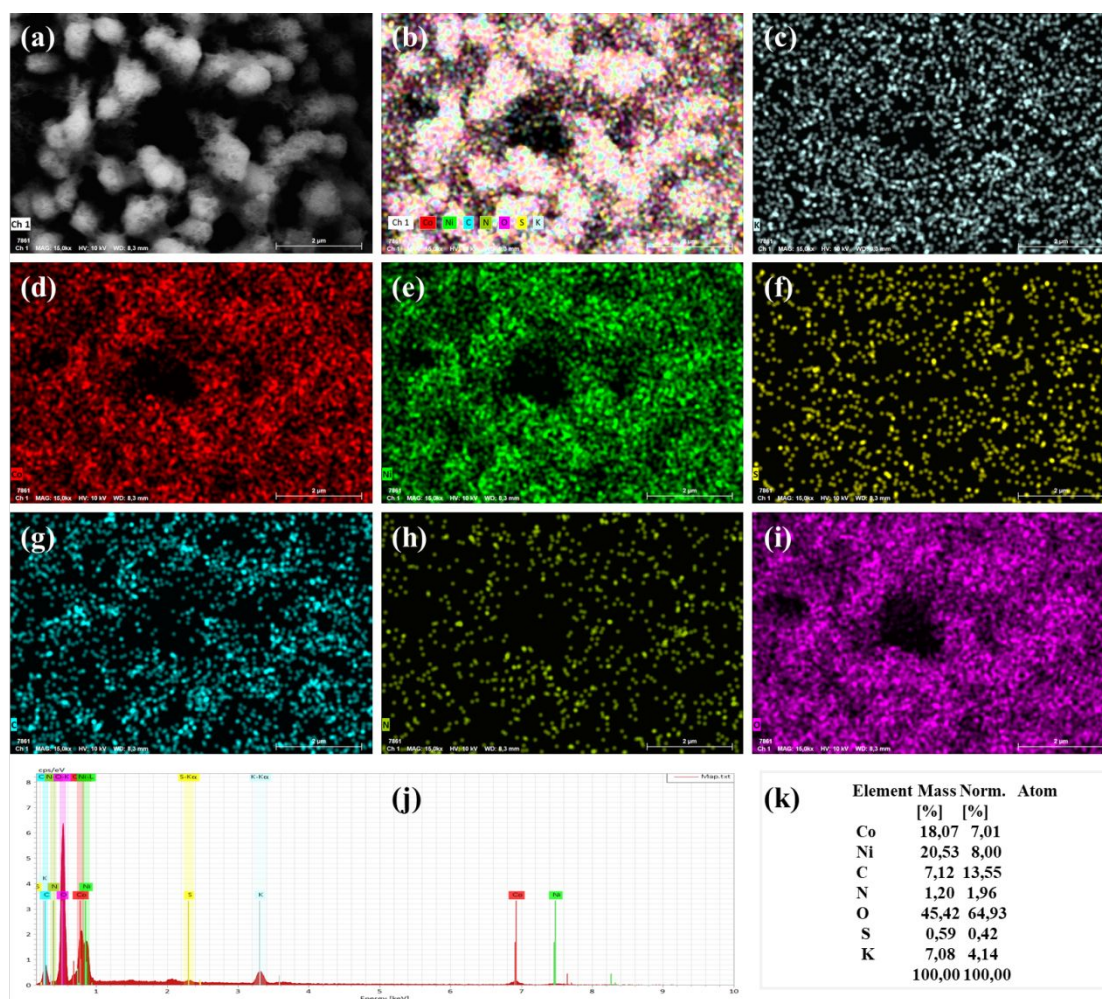**Fig. S2-2.** FESEM element mapping and energy spectrum of the optimal sample (NiCo-S@CNFs).

**Fig. S2-4.** FESEM element mapping and energy spectrum of the optimal sample (NiCo-S@CNFs)

after durability test.

4. Capacitance fluctuation can be observed in Fig. 7i, so the authors should justify it

with proper reason.

**Response:**

Thank you for your question. After 12,000 cycles of GCD (**Figure 7(i)**), the capacity

retention rate remained at 105.1% of the initial capacity. The built-in graph displayed

comparison curves of GCD (1st-5th, 5995th-6000th, and 11996th-12000th), the trend

of increasing first and then leveling off indicates the process of activation and stable

operation of the HSC. The main reason for the capacity retention rate to be greater than 100% is that the material gradually activates with the accumulation of the number of cycles, so it slightly exceeds 100%. The ultra-high cycle retention rate of 104.5% after 12000 cycles can be achieved, which is mainly attributed to the material structure and the stability of the substance in the electrolyte. Fluctuations in the cycle can be attributed to the volatilization (replenishment) of electrolytes and temperature changes. After carefully studying the experimental process and related data, and consulting some related documents, we analyze and summarize the following reasons. Generally, the GCD cycle process is accompanied by the continuous activation of the electrode material in the HSC, so the capacity of the device will increase to a certain extent as the number of cycles increases. However, as the number of cycles continues to accumulate, an equilibrium state is finally reached. In fact, in the process of cyclic accumulation, the electrolyte will gradually be consumed (decomposition, volatilization, or participating in the reaction, and there will be a concentration change). The above phenomenon is very easy to cause the capacity of HSC to change and fluctuate to a certain extent, and there is a high probability that it will show a downward trend. Especially because the room temperature is higher in summer and the cycle time is longer, the change of electrolyte will become more obvious, which leads to this problem. Therefore, we think that the cycling stability of the NiCo-S@CNFs-based supercapacitor over 12000 cycles will be a gradual and regular decline.

5. In the evaluation of electrochemical performance, the study of electrochemical impedance is equally important, and the author should further describe and improve the resistance value of the data.

**Response:**

Thanks very much for your suggestion. We agree that the study of electrochemical impedance is equally important. Besides, we have supplemented the relevant descriptions in the manuscript and added the relevant data summary table in the supplementary materials. and the resistance value of the data. The supplementary summary table is as follows：

**Table S7.** The EIS fitted data for all the EIS graphs.

| Samples | $R_s$ (ohm) | $R_{ct}$ (ohm) |
|---|---|---|
| NiCo-S-100-2 | 1.31 | 0.08 |
| NiCo-S-100-1 | 3.31 | 0.72 |
| NiCo-S-100-3 | 2.47 | 0.13 |
| NiCo-S-50-2 | 1.45 | 0.16 |
| NiCo-S-150-2 | 1.39 | 0.31 |
| NiCo 1:2-200s-S | 1.21 | 0.42 |
| NiCo 1:2-400s-S | 1.32 | 0.20 |
| NiCo 1:1-300s-S | 1.25 | 0.08 |
| NiCo 1:0-300s-S | 1.54 | 0.43 |
| CoZ1D-NiCo-LDH | 3.38 | 0.11 |
| CoZ1D | 1.38 | 0.08 |

| | | |
|---|---|---|
| CoZ1D-S | 1.21 | 0.07 |
| CC-NiCo-LDH | 1.37 | 0.13 |
| CC-NiCo-LDH-S | 1.30 | 0.07 |
| AC | 0.72 | 0.45 |
| HSC | 1.56 | 0.35 |

6. To better explain the electrodes' high performance and stability, the authors should conduct a more in-depth analysis of their electrochemical properties.

**Response:**

Thanks very much for your suggestion. We agree that a more in-depth analysis of the electrochemical properties of the electrodes can better explain the high performance and stability of the electrodes. Therefore, we consulted more literature and further analyzed the reaction mechanism to supplement and correct the redox reaction of multiphase electrode materials in alkaline electrolyte KOH, and the relevant content has been added and corrected in the manuscript. In this work, the existing physical characterization and data are further analyzed, and the electrode element mapping and EDS spectra after the durability test are supplemented. The relevant contents have been supplemented in the manuscript and supplementary materials.

7. The background discussion on transition metal sulfides and hybrid supercapacitors is well-written but incomplete. Recent works on advanced energy storage materials, such as heterostructured and hierarchical composites for supercapacitors, should be included to position the study more effectively. Some references may be helpful:

DOI:10.1016/j.jcis.2021.12.159;  DOI:10.1007/s40843-020-1476-2.

**Response:**

Thank you very much for your suggestion. We agree that some recent related works on heterostructured and hierarchical composites for supercapacitors should be cited and discussed appropriately. The references can provide us with better guidance in the fields of supercapacitors, design strategies, and further energy storage mechanisms of high-performance electrodes. In addition, the supplement of relevant references makes our manuscript perfect. We have added them to the manuscript for theoretical support. Thank you again for your suggestion.